Earth's Future

RESEARCH ARTICLE
10.1029/2025EF006108

Projections of Lightning-Ignited Wildfire Risk in the Western United States

Dmitri A. Kalashnikov[1,2], John T. Abatzoglou[3], Frances V. Davenport[4], Zachary M. Labe[5], Paul C. Loikith[6,7], Danielle Touma[8], and Deepti Singh[2]

[1]Sierra Nevada Research Institute, University of California, Merced, CA, USA, [2]School of the Environment, Washington State University, Vancouver, WA, USA, [3]Management of Complex Systems Department, University of California, Merced, CA, USA, [4]Civil and Environmental Engineering, Colorado State University, Fort Collins, CO, USA, [5]NOAA/OAR/Geophysical Fluid Dynamics Laboratory, Princeton, NJ, USA, [6]Department of Geography, Portland State University, Portland, OR, USA, [7]Institute for Sustainable Solutions, Portland State University, Portland, OR, USA, [8]Institute for Geophysics, University of Texas at Austin, Austin, TX, USA

Abstract Cloud-to-ground (CG) lightning is a major source of summer wildfire ignition in the western United States (WUS). However, future projections of lightning are uncertain since lightning is not directly simulated by most global climate models. To address this issue, we use convolutional neural network (CNN)-based parameterizations of daily June-September CG lightning. CNN parameterizations of daily CG lightning occurrence at each grid cell use fields of three thermodynamic variables—ratio of surface Moist Static Energy (MSE) to 500 hPa saturation MSE, 700–500 hPa lapse rate, and 500 hPa relative humidity. Applying these parameterizations to the Community Earth System Model version 2 Large Ensemble, we find widespread increases in CG lightning days across much of the region by the mid-21st century (2031–2060) under a moderate warming scenario. Projected increases are pronounced in the northern WUS where many grid cells experience 4–12 additional CG lightning days compared to 1995–2022 and are driven by increases in all three thermodynamic variables. To assess the risk of lightning-ignited wildfire (LIW) ignition, we also quantify the concurrence of CG lightning with high Fire Weather Index (FWI) days. By 2031–2060, CG lightning will coincide more frequently with high FWI, but the magnitude of increases relative to CG lightning days varies across the region. Future projections of CG lightning and LIW risk can be useful for understanding the changing risks of associated hazards, and guide wildland fire management and suppression planning.

Plain Language Summary Cloud-to-ground lightning is a major source of wildfire ignition during the summer in the western United States, but future projections of lightning and lightning-ignited wildfire (LIW) have been limited. We use a machine learning technique—convolutional neural networks–to predict lightning based on three meteorological variables. These variables describe aspects of atmospheric moisture and vertical instability and therefore capture conditions favorable for lightning occurrence. We then apply these machine learning-based models to output from GCM simulations to project cloud-to-ground lightning days in the future. Our projections show an increase in cloud-to-ground lightning days in the mid-21st century (2031–2060), especially in the interior northwestern United States. These increases are driven by widespread projected increases in all three meteorological variables used for lightning prediction. We also project an increased likelihood of cloud-to-ground lightning occurring on days with meteorological conditions favorable for wildfires, thus increasing the risk of LIWs. These findings are important for understanding changes to LIW risk, and for planning wildland fire management and suppression needs in a warming climate.

Key Points:

- Increases in cloud-to-ground lightning days are projected across the western U.S. in CESM2-LENS2, particularly in the interior Northwest
- Increases in lightning are driven by rises in moisture and instability indices used for convolutional neural network-based lightning models
- Lightning-ignited wildfire risk grows as high Fire Weather Index days increasingly align with lightning days

Supporting Information:

Supporting Information may be found in the online version of this article.

Correspondence to:

D. A. Kalashnikov,
dkalashnikov@ucmerced.edu

Citation:

Kalashnikov, D. A., Abatzoglou, J. T., Davenport, F. V., Labe, Z. M., Loikith, P. C., Touma, D., & Singh, D. (2025). Projections of lightning-ignited wildfire risk in the western United States. *Earth's Future*, *13*, e2025EF006108. https://doi.org/10.1029/2025EF006108

Received 7 FEB 2025
Accepted 15 JUL 2025

Author Contributions:

Conceptualization: Dmitri A. Kalashnikov, John T. Abatzoglou, Deepti Singh
Data curation: Danielle Touma
Formal analysis: Dmitri A. Kalashnikov
Funding acquisition: Dmitri A. Kalashnikov, Deepti Singh
Investigation: Dmitri A. Kalashnikov
Methodology: Dmitri A. Kalashnikov, John T. Abatzoglou, Frances V. Davenport, Zachary M. Labe, Paul C. Loikith, Danielle Touma, Deepti Singh
Project administration: Deepti Singh
Resources: Dmitri A. Kalashnikov, John T. Abatzoglou, Deepti Singh
Software: Dmitri A. Kalashnikov
Supervision: John T. Abatzoglou, Deepti Singh

1. Introduction

In the western United States (WUS), wildfires ignited by cloud-to-ground (CG) lightning during the summer are responsible for more than two-thirds of the total burned area (Abatzoglou et al., 2016). Smoke from these fires has detrimental effects on air quality and public health and has partially reversed air quality improvements stemming from the Clean Air Act (Burke et al., 2023; Kalashnikov, Schnell, et al., 2022; J. Liu et al., 2016; McClure & Jaffe, 2018; D. Zhang et al., 2023). As the climate continues to warm in the WUS, the risk of wildfires—including those sparked by lightning—is projected to grow due to drier vegetation (Abatzoglou, Battisti, et al., 2021; Brown et al., 2021; Li et al., 2020; McGinnis et al., 2023; Pérez-Invernón et al., 2023). Furthermore, recent research indicates that lightning could become more frequent in parts of the globe (Janssen et al., 2023; Pérez-Invernón

Validation: Dmitri A. Kalashnikov
Visualization: Dmitri A. Kalashnikov
Writing – original draft: Dmitri A. Kalashnikov
Writing – review & editing: Dmitri A. Kalashnikov, John T. Abatzoglou, Frances V. Davenport, Zachary M. Labe, Paul C. Loikith, Danielle Touma, Deepti Singh

et al., 2023; Whaley et al., 2024), amplifying the risk of increased wildfire activity. These projections underscore the need to understand and prepare for the potential societal and environmental consequences of increased wildfire activity. In addition to wildfire risk assessments, understanding changes to CG lightning is also crucial as it poses direct risks to human safety and infrastructure.

Most state-of-the-art global climate models (GCMs) are unable to directly simulate lightning because their coarse spatial resolution prevents them from capturing the fine-scale physical processes involved in lightning production. To project future lightning, previous studies have relied on convective parameterizations, using proximal variables like cloud top height, convective ice and mass flux, or the product of convective available potential energy (CAPE) and precipitation rate (Allen & Pickering, 2002; Chen et al., 2021; Finney et al., 2018; Janssen et al., 2023; Magi, 2015; Pérez-Invernón et al., 2023; Price & Rind, 1992; Romps et al., 2014). Projections have been shown to vary substantially depending on the specific parameterization used and the microphysics scheme of the GCM, leading to uncertainty in the potential changes to future lightning activity (Charn & Parishani, 2021; Clark et al., 2017; Etten-Bohm et al., 2024; Romps, 2019). To overcome these limitations, recent studies have also developed simpler lightning parameterizations based on large-scale meteorological variables that are directly simulated by GCMs, employing methods such as logistic regression (Etten-Bohm et al., 2021, 2024; Whaley et al., 2024), random forests (N. Liu et al., 2022), and neural networks (Cheng et al., 2024; Kalashnikov et al., 2024; Verjans & Franzke, 2025).

However, most parameterizations have been derived from lightning observations in the global tropics and subtropics where the necessary ingredients for convection may differ in importance compared to the WUS, potentially introducing biases when applied over this region. The WUS is a region of complex terrain and is additionally represented by more than one distinct lightning regime. For example, lightning tends to occur in conjunction with deep convection in the North American Monsoon (NAM) core region of the interior Southwest. On the other hand, areas on the NAM periphery are prone to "dry" lightning, which occurs under specific atmospheric conditions (e.g., mid-level moisture overlying a dry lower troposphere) that may not be captured by parameterizations developed at national to global scales (Kalashnikov, Abatzoglou, et al., 2022; Nauslar et al., 2013; Rorig & Ferguson, 1999). Importantly, widely-used lightning parameterizations such as the product of CAPE and the precipitation rate of Romps et al. (2014) may not capture dry lightning, as dry lightning can occur without high surface-based CAPE or heavy precipitation.

To develop local parameterizations that address these gaps, we employ Convolutional Neural Network (CNN)-based CG lightning parameterizations developed in Kalashnikov et al. (2024) that were trained at individual $1° \times 1°$ grid cells of the WUS to project CG lightning days for 2031–2060 across this region. To identify the key environmental factors driving projected changes in CG lightning, we also interrogate changes in atmospheric circulation and the thermodynamic fields used for lightning prediction. Prior to Kalashnikov et al. (2024), lightning parameterizations targeted for the WUS, whether based on convective parameters or the large-scale environment, were lacking. As our parameterizations were developed by training models at individual grid cells, we account for localized conditions conducive to lightning formation. The CNNs were also explicitly designed to model CG lightning, as CG lightning is uniquely capable of igniting wildfires due to its direct contact with the ground. Importantly, to the best of our knowledge our analysis is the first to leverage large ensemble climate simulations to understand future trajectories of these risks across the WUS and their uncertainty due to internal climate variability.

However, CG lightning by itself may not pose a risk of wildfire ignition if accompanied by heavy rainfall or contacting wet fuels (Alexander, 1927; Rao et al., 2023). Indeed, previous studies show only a weak correlation between interannual WUS burned area and lightning activity (e.g., Abatzoglou et al., 2016). To better understand the future risk of lightning-ignited wildfires (LIWs), it is critical to consider the concurrence of CG lightning and weather conditions that enable wildfire ignition and spread. Studies that have explicitly accounted for wildfire drivers in combination with lightning projections have been limited and represent an emerging area of research (Krause et al., 2014; Pérez-Invernón et al., 2023; Price & Rind, 1994; Whaley et al., 2024). Thus, we also quantify changes in the Fire Weather Index (FWI; Wagner, 1987), which serves as a proxy for the meteorological and climatic conditions conducive to ignitions and large wildfire activity across different biomes (Barbero et al., 2014; Di Giuseppe et al., 2018; Urbieta et al., 2015) and their intersection with CG lightning days.

2. Data and Methods

2.1. Convolutional Neural Networks

In Kalashnikov et al. (2024), we trained individual CNNs at each 1° × 1° grid cell of the conterminous WUS (initial number of CNNs trained = 285) to predict the daily occurrence (≥1 CG flash) or non-occurrence of CG lightning at that grid cell. CNNs are well-suited for capturing complex and non-linear relationships in geophysical phenomena (Baño-Medina et al., 2021; Molina et al., 2021, 2023; Toms et al., 2020). The CNNs were trained using meteorological data from the National Aeronautics and Space Administration's (NASA) Modern-Era Retrospective Analysis for Research and Applications, Version 2 (MERRA-2; 0.5° × 0.625°) (Gelaro et al., 2017) as predictor variables and CG lightning data from the National Lightning Detection Network (NLDN; 0.1° × 0.1°) as the response variable over June–September 1995–2022 (hereafter, "warm season"). We focus our analysis on the warm season since it captures the vast majority of WUS lightning activity and wildfire burned area, and provides a relatively consistent set of summertime lightning-producing meteorological patterns for CNN training (Abolafia-Rosenzweig et al., 2022; Kalashnikov et al., 2020). Both data sets were upscaled to 1° × 1° resolution: MERRA-2 via bilinear interpolation and NLDN by counting any CG lightning observed within constituent 0.1° grid cells as a lightning day in the overlying 1° grid cell. The 1° spatial resolution was chosen to be compatible with current state-of-the-art GCMs and to reduce computational cost during CNN training. Daily fields of these meteorological variables (see Section 2.2) were interpolated to equal-area 20 × 20 grids spanning 2000 km on each side (100 km × 100 km resolution) and centered on each grid cell for local CNN training. Important spatial features in adjacent and upwind regions contribute useful information for prediction, and CNNs learn to effectively ignore irrelevant features during training (Baño-Medina et al., 2021; Kalashnikov et al., 2024).

In this study, we utilize the reduced three-predictor CNNs from Kalashnikov et al. (2024) due to lower computational cost and similar performance to the more complex CNNs tested in that study (see Figure S3 in Supporting Information S1 therein). Therefore, for each day, the input to each local CNN is a three-dimensional matrix of size 20 latitude × 20 longitude × 3 input variables. The CNN architecture comprises two convolutional layers with 3 × 3 filters, each followed by a max pooling layer with 2 × 2 filters, and the output is passed to a dense layer with 16 neurons. We use He uniform initialization (He et al., 2015) and Rectified Linear Unit activation in the convolutional and first dense layer. Inputs are then vectorized and sent to a classification layer with two neurons and a Softmax activation function, producing continuous probabilities (ranging from 0 to 1) for each classification: CG lightning or non-lightning. Days with model-predicted CG lightning probabilities >0.5 are classified as CG lightning days. We refer the reader to Kalashnikov et al. (2024) for additional details about CNN architecture, hyperparameter tuning, and training. The CNNs were developed using TensorFlow 2.11.1 in Python (Abadi et al., 2015).

2.2. Meteorological Variables

The three thermodynamic variables used for CG lightning prediction are the ratio of surface moist static energy (MSE) to the saturation MSE at 500 hPa (MSE_{ratio}), representing a simple convective proxy wherein a value of >1 indicates a likelihood that ascending air parcels will saturate and condense (Noyelle et al., 2023; Y. Zhang & Boos, 2023); the vertical temperature difference or lapse rate between the 700 and 500 hPa pressure levels ($\Gamma_{700–500}$), with larger values indicating increased buoyancy for vertical ascent that can invigorate convection; and the relative humidity at 500 hPa (RH_{500}) which captures the degree of saturation at that level. These variables parsimoniously capture three-dimensional temperature and moisture information relevant for lightning formation. Furthermore, these variables are expected to be reasonably climate-invariant, that is, their physical relationship with lightning should be generalizable to a future, warmer climate (Beucler et al., 2024). This is accomplished through the use of relative quantities such as MSE_{ratio} and RH_{500} rather than absolute quantities such as column water vapor or specific humidity, as the predictive relationship of the latter may shift with warming. For example, convection may not increase in the future despite increasing lower-tropospheric moisture if the saturation profile remains constant (Beucler et al., 2024; Pascale et al., 2018). However, we note that other tropospheric changes may affect the predictive relationship between the chosen variables and future lightning activity, including changes to near-surface instability or cloud microphysical shifts that could alter lightning production (Clark et al., 2017).

2.3. Climate Model Simulations

For projections of lightning days, corresponding variables are obtained or derived from the Community Earth System Model v2 Large Ensemble (CESM2-LENS2; hereafter, CESM2) (Danabasoglu et al., 2020; Rodgers et al., 2021) that uses CMIP6 historical forcings until 2014 and the SSP3-7.0 scenario for 2015–2100. Single model initial-condition large ensembles are useful for quantifying uncertainties in projections of CG lightning, LIW risk, and the predictor variables due to irreducible internal climate variability (Deser et al., 2012; Lehner et al., 2020; Tebaldi et al., 2021). Additionally, CESM2 has shown improvement in simulating NAM precipitation over CESM1 (Meehl, Shields, et al., 2020). CESM2 includes 100 ensemble members with identical external forcings except for biomass burning emissions, which are from CMIP6 for the first 50 members and smoothed for the last 50 members. We use the 50 members with time-varying CMIP6 biomass burning emissions to maintain consistency of forcings.

The CESM2 variables used are T500 (T_{500} herein), T700 (T_{700}), and Q500 for the computation of $\Gamma_{700–500}$ and RH_{500}. To derive the MSE_{ratio}, we use 2-m temperature (TREFHT; T_{2M} herein), 2-m specific humidity (QREFHT; Q_{2M}), geopotential height at the surface (PHIS) and 500 hPa (Z500; Z_{500}), and T500. To diagnose accompanying changes in atmospheric circulation, we use Z_{500} and 500-hPa winds (WS_{500}) obtained from u and v winds at that level (U500 and V500, respectively). We examine both raw Z_{500} and its standardized anomalies (i.e., z-scores), computed from 15-day windows centered on each day during 1995–2022 and 2031–2060. Standardized anomalies are calculated for each period separately to account for tropospheric expansion from background warming. We also quantify changes in the frequency of "ridge breakdown" patterns, which occur when a high-pressure ridge over the interior WUS is weakened and displaced by an incoming mid-latitude disturbance. These patterns have long been associated with high fire danger, as incoming cold air aloft overrides residual warm air near the surface to create instability sufficient for convection, while mid-level moisture and dry air at lower levels promote the formation of dry lightning (Abatzoglou & Brown, 2009; Kalashnikov et al., 2020; Werth & Ochoa, 1993). Ridge breakdown events are identified at each grid cell where a Z_{500} anomaly $>1\sigma$ is followed within three days by a $<-0.5\sigma$ anomaly.

CESM2 variables are regridded from their native resolution ($0.94° \times 1.25°$) to match the $1° \times 1°$ resolution of the trained CNNs using bilinear interpolation. All CESM2 maps show the ensemble mean. Results are considered robust if >75% of ensemble members (at least $n = 38$) agree on the projected sign of change.

2.4. Bias Correction of Predictor Variables

Mean fields of the CESM2 predictor variables were evaluated over the 1995–2022 warm seasons for biases compared to MERRA-2, and all three variables were found to exhibit varying degrees of biases across the WUS (not shown). As these biases might affect prediction accuracy, we apply a multivariate bias-correction procedure to the predictor variables prior their use as inputs to the CNNs. Multivariate bias correction, rather than the more commonly used univariate approach, is preferable because the CNNs were trained on the predictor variables as a single input matrix. Therefore, they likely learned to predict CG lightning based on the combined information of the three predictors, including their individual spatial fields and multivariate dependence. We employ the "MBCn" procedure from Cannon (2018), which is a multivariate generalization of quantile mapping for climate variables based on the image transfer algorithm developed by Pitie et al. (2005). This procedure adjusts the univariate quantiles of each CESM2 variable using quantile delta mapping (Cannon et al., 2015), and further adjusts their multivariate distribution toward MERRA-2 (the historical baseline for calibration), while preserving trends in the climate model data (Cannon, 2018). We first bias-correct one randomly selected ensemble member, then apply those quantiles to all 50 members. This removes only the CESM2 model biases while preserving the natural variability in the ensemble spread (Cannon et al., 2022; Kirchmeier-Young et al., 2017). The remaining biases in the individual variables and their covariance are substantially reduced (not shown). The MBCn algorithm is implemented using the xclim Python package (version 0.50.0; Bourgault et al., 2023).

Bias-corrected meteorological variables from CESM2 are interpolated following the approach described in Section 2.1 to create $20 \times 20 \times 3$ input matrices for each day across all ensemble members. Prior to input, the CESM2 predictor variables are rescaled by the maximum values of the corresponding MERRA-2 data sets used for CNN training. This preserves absolute changes in the rescaled predictor values between historical and future climates. The trained CNN models are then applied to predict the occurrence of CG lightning at each corresponding $1° \times 1°$ grid cell using CESM2 data.

2.5. Wildfire Ignition Risk

We use the FWI from the Canadian Forest Fire Danger Rating System to quantify LIW risk on projected CG lightning days. The FWI is a widely-used index for quantifying potential wildland fire ignition and spread that accounts for both weather and antecedent climatic conditions. It is typically calculated from meteorological variables at noon local time for operational forecasting. However, due to the barriers in obtaining climate model data at noon local time, we use daily values of these variables following previous work (Abatzoglou et al., 2019; Gallo et al., 2023; Touma et al., 2022). We calculate the FWI over the historical period using daily maximum temperature, daily accumulated precipitation, daily minimum relative humidity, and daily-average 10-m wind speed data from MERRA-2 using the xclim Python package. Similarly, the FWI is computed using the following CESM2 variables: 2-m maximum temperature (TREFHTMX), total precipitation (PRECT), daily-minimum 2-m relative humidity (RHREFHT; RH_{2M} herein), and 10-m wind speed (U10).

Previous studies have used FWI percentiles (e.g., 95th or 99.9th) to project wildland fire potential (Abatzoglou et al., 2019; Abatzoglou, Juang, et al., 2021; Goss et al., 2020; Touma et al., 2022, 2023). While this is a valid approach that considers extreme fire danger from an atmospheric perspective, a potential limitation is that vegetation and climate-dependent differences in ignition-relevant FWI thresholds are not considered. We refine this approach by identifying empirical FWI thresholds associated with historical LIW ignitions within Bailey's ecoprovinces (USFS, 1995). Bailey's ecoprovinces are regions of broadly similar climate, vegetation characteristics, and climate-fire dynamics and have proven useful for partitioning the WUS in prior LIW analyses (Abatzoglou et al., 2016; Kalashnikov et al., 2023).

Wildfire data are sourced from the Fire Program Analysis Fire-Occurrence Database that documents all wildfires from federal, state, and local reporting agencies in the United States between 1992 and 2020 (Short, 2022). We select fires labeled as "natural" that attained a final burned area >1 ha (Fusco et al., 2019; Kalashnikov et al., 2023) during the 1995–2020 warm seasons. Fire latitude, longitude, and discovery dates are then used to aggregate fire occurrence to daily presence/absence of wildfire discovery at each 1° × 1° grid cell. However, the fire discovery date may not represent the actual ignition date in the case of holdover fires, which can smolder undetected for days (Kalashnikov et al., 2023; Schultz et al., 2019). We therefore conduct a backward search for CG lightning at each 1° × 1° grid cell, starting on days with reported fire discovery and searching up to a maximum of 5 days prior (Kalashnikov et al., 2023). The closest temporal occurrence of CG lightning prior to the fire discovery date is considered the LIW ignition day for which the FWI value is extracted. We acknowledge that this approach may not accurately capture all ignition dates given the uncertainty in the timing and placement of CG lightning relative to ignition locations, and the potential for meteorological and environmental conditions to enable longer-lived holdover fires that ignited prior to the 5-day search window (Schultz et al., 2019). Nonetheless, this approach provides a reasonable approximation of the most recent CG lightning activity prior to fire discovery.

For each ecoprovince, FWI values from all ignition days (i.e., when CG lightning was observed rather than when the fire was discovered) at constituent grid cells are aggregated into a single distribution, and the ecoprovince-median value is calculated. As a final step, FWI percentiles (calculated from the warm-season distribution) that correspond to these median values are computed (Figure S1 in Supporting Information S1). LIWs in all ecoprovinces ignite with median FWI values between the ∼36th–71st percentiles of the warm-season distribution (Figure S1 in Supporting Information S1). We thus note that substantial LIW ignition risk exists at non-extreme FWI values, likely due to precipitation and humidity that typically accompany thunderstorms that lead to short-term declines in FWI (Barros et al., 2021). Exceedances of these ecoprovince-specific FWI percentiles are identified in CESM2 output. If co-occurring with predicted CG lightning, such exceedances are termed "LIW-risk days" that signal a greater risk of LIW ignition where sufficient fuels are available. We also quantify the "LIW-risk fraction," defined as the ratio of LIW-risk days to the total number of CG lightning days, with a higher fraction indicating more frequent co-occurrence of CG lightning days with fire-conducive FWI.

2.6. Domain Selection

Our study domain is the conterminous WUS. We start with the 285 1° × 1° grid cells for which CNNs were trained in Kalashnikov et al. (2024). This initial domain extended from 32 to 49°N latitude and from the Pacific Ocean to 104°W longitude and excluded grid cells that experience CG lightning on less than 10% of warm-season days, as the small sample sizes were suboptimal for CNN training (see Figure 1 in Kalashnikov et al., 2024). Next, we

10.1029/2025EF006108

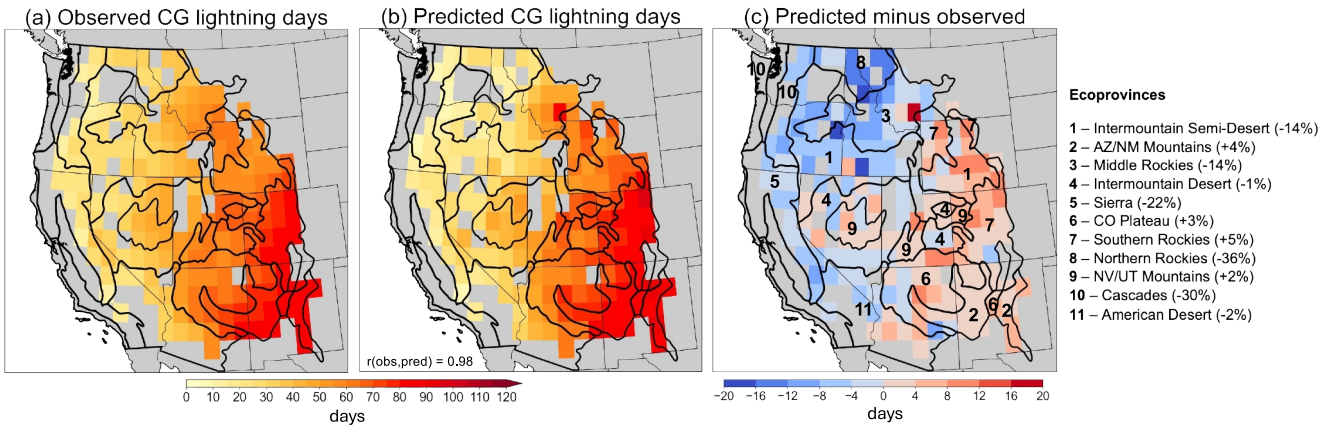

Figure 1. (a) Observed seasonal-average number of days with at least one cloud-to-ground (CG) lightning flash in 1° × 1° grid cells during June-September (1995–2022) from the National Lightning Detection Network, and (b) predicted number of CG lightning days using convolutional neural networks applied to CESM2, obtained from the average of 50 ensemble members. Inset text in (b) is the spatial correlation between observed and predicted CG lightning days. (c) Biases in CG lightning days between observations and CESM2 predictions. Ecoprovince names are provided in adjoining table along with percentage biases between observations and predictions for each ecoprovince.

exclude grid cells with low CNN classification performance. These locations exhibit either a precision-recall Area Under the Curve of <0.5 (i.e., no classifications skill), or prediction bias exceeding ±25% of total CG lightning days when applied to MERRA-2 and compared to NLDN observations over the historical period. We assign the remaining grid cells into the 11 Bailey's ecoprovinces that are fully contained within the WUS and experience meaningful LIW activity (Figure 1) (Kalashnikov et al., 2023). Grid cells are assigned if >50% of their area belongs to that ecoprovince. To ensure that all remaining grid cells can experience impactful wildfires, we apply a burnable/unburnable mask using the Global Land Data Assimilation System vegetation classes. Grid cells with dominant vegetation classes consisting of "Permanent Wetland," "Cropland," "Urban and Built-Up," "Cropland/Natural Vegetation Mosaic," "Snow and Ice," or "Barren or Sparsely Vegetated" are considered unburnable as they rarely foster LIWs and are therefore excluded from analysis, while all other grid cells are considered burnable. We focus our analyses on the 193 retained grid cells with consequential CG lightning and LIW activity in the WUS, and where CG lightning can be reliably predicted by the CNNs (Figure 1).

3. Results

3.1. Evaluation of CG Lightning Parameterizations

The locally-trained CNN-based lightning parameterizations over the CESM2 model years 1995–2022 reproduce the observed spatial patterns of warm-season CG lightning days across the WUS with high fidelity, with a spatial correlation coefficient of $r = 0.98$ between observations and predictions (Figures 1a and 1b). The CNNs capture the northwest to southeast gradient of increasing lightning activity, particularly associated with the NAM core region. Biases between observed and CESM2-simulated CG lightning days are present across most of the domain but are within 36% in all ecoprovinces (Figure 1c). Negative biases are found in the Northwest, where CNNs predict >12 fewer CG lightning days per warm season in some locations in Idaho, eastern Oregon, and western Montana. Conversely, positive biases of 4–12 CG lightning days are found over southeastern parts of the WUS. However, due to the climatologically larger number of CG lightning days within the NAM core region, positive biases do not exceed 5% in any ecoprovince (Figure 1c). CESM2 also reproduces the observed climatology of LIW-risk days (spatial correlation coefficient $r = 0.94$), which follow the same spatial pattern as CG lightning days but occur about one-third as frequently across the WUS (Figure S2 in Supporting Information S1). Underpredictions are prevalent throughout the WUS except for Arizona and New Mexico (Figure S2c in Supporting Information S1).

3.2. CESM2 Projections of CG Lightning and LIW-Risk Days

Next, we quantify mid-21st century projections (2031–2060) of CG lightning and LIW-risk days in CESM2, and report widespread increases across the WUS relative to the historical period (1995–2022; Figures 2a and 2b).

10.1029/2025EF006108

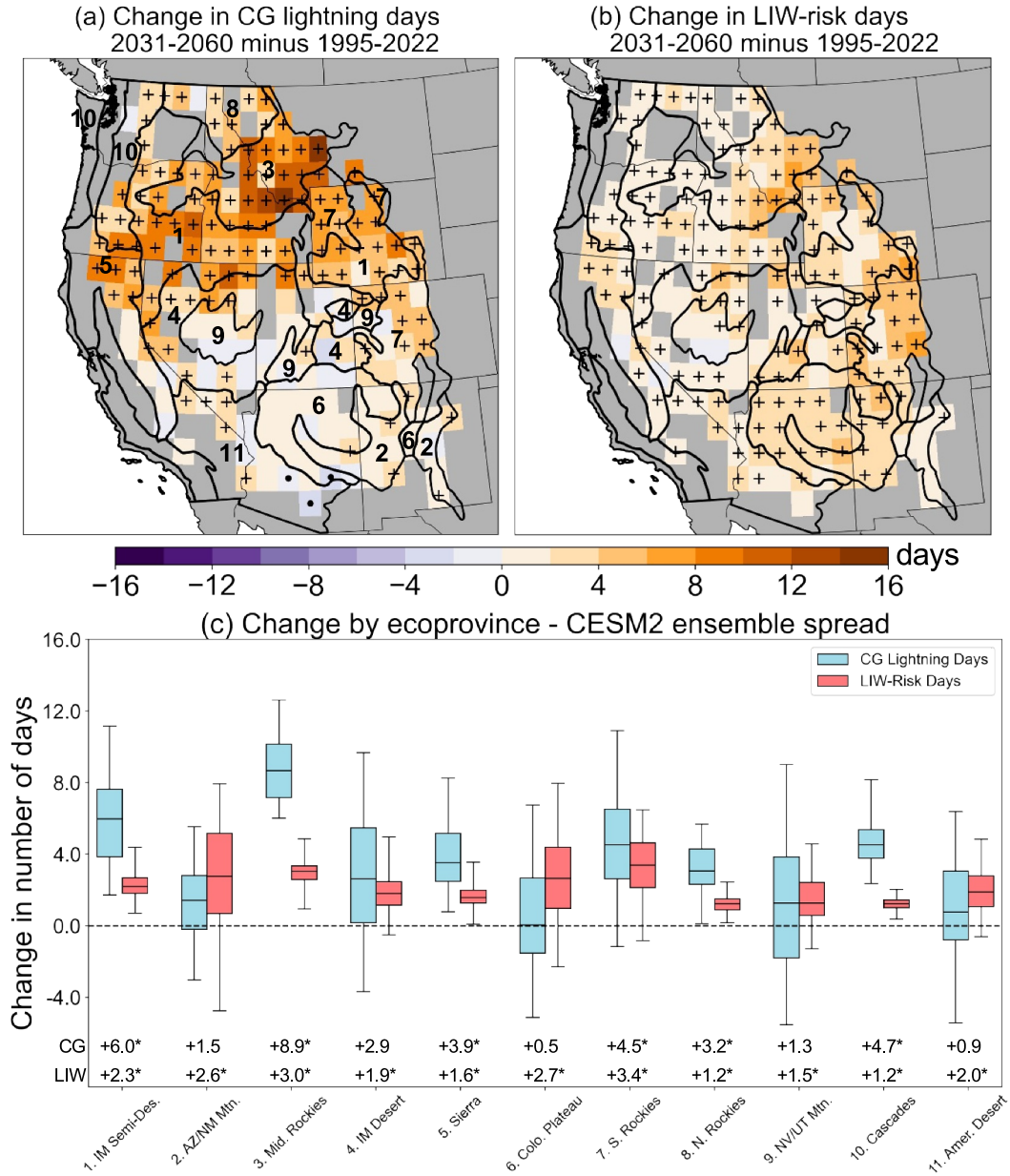

Figure 2. Ensemble-mean projected changes in (a) CG lightning days and (b) LIW-risk days between historical (1995–2022) and mid-century (2031–2060) periods during June-September. Plus signs (dots) indicate where >75% of ensemble members agree on increases (decreases). (c) CESM2 ensemble distribution of projected changes in CG lightning and LIW-risk days averaged across ecoprovinces. Horizontal lines within boxplots indicate medians and whiskers represent spread of the 50 ensemble members. Ecoprovince numbers in (c) correspond to numeric labels in (a). Text along bottom of (c) shows ensemble-mean changes, with * indicating that a majority of grid cells have >75% ensemble agreement on the sign of change in that ecoprovince.

Increases in CG lightning days are robust (>75% ensemble agreement) across the northern half of the domain, suggesting these increases are likely even after accounting for internal climate variability (Figure 2a). Increases are especially pronounced across the Middle Rockies (+8.9 days), Intermountain Semi-Desert (+6.0 days), and Cascades (+4.7 days) ecoprovinces (Figures 2a and 2c). Meanwhile, projected increases are generally weak and not robust across the southern half of the domain. In contrast to the spatial variations in CG lightning days, projected increases in LIW-risk days are ubiquitous (~98% of grid cells) and robust across nearly the entire

10.1029/2025EF006108

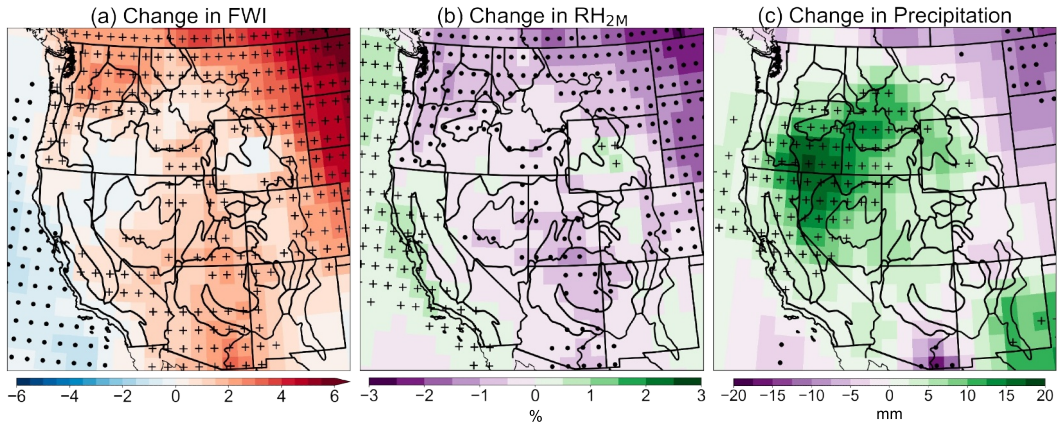

Figure 3. Ensemble-mean changes in: (a) Fire Weather Index and two key components of the FWI: (b) 2-m relative humidity (RH_{2M}), and (c) precipitation between historical (1995–2022) and mid-century (2031–2060) during June-September. Plus signs (dots) indicate where >75% of ensemble members agree on increases (decreases).

domain, but are most pronounced in eastern parts including the Southern Rockies (+3.4 days) and Middle Rockies (+3.0 days) (Figures 2b and 2c).

Notably, many grid cells in Utah and Arizona that see non-robust increases or even decreases in CG lightning days are projected to experience more LIW-risk days due to increases in FWI (Figures 2c and 3a). Conversely, many northern areas will see smaller increases in LIW-risk days compared to increases in CG lightning days due to only modest increases and even decreases in FWI especially in parts of the Intermountain Semi-Desert ecoprovince, that are in turn driven by increases in warm-season precipitation (Figures 3a and 3c). The Middle Rockies are another example, with simulated changes of +8.9 CG lightning days but only +3.0 LIW-risk days per warm season (Figure 2c). Nevertheless, most of the WUS, or ∼92% of grid cells, is projected to see increases in the LIW-risk fraction (defined as the ratio of LIW-risk days to overall CG lightning days) compared to 1995–2022 due to widespread increases in FWI during the warm season (Figures 3a and 4). FWI increases are a byproduct of increasing T_{2M} and decreasing RH_{2M} (Figure 3b, Figure S3c in Supporting Information S1), consistent with other projections for this region (e.g., Abatzoglou et al., 2019; Yu et al., 2023). Increases in the LIW-risk fraction suggest that CG lightning is more likely to produce LIWs in the future relative to present climate. Increases are robust across many areas, with a notable exception being the western Great Basin where some grid cells project a decline in the LIW-risk fraction by mid-century. These locations show robust increases in warm-season precipitation of 5–20 mm and consequent decreases in FWI despite warming T_{2M} of 1.5–2.5°C (Figures 3a and 3c, Figure S3c in Supporting Information S1). Coupled with a simultaneous increase in overall CG lightning days (Figure 2a), these trajectories are consistent with a possible extension of the NAM monsoonal anticyclone northwestward from its present-day position (Pascale et al., 2018; see also Section 3.3).

When looking at the monthly scale, projected CG lightning increases are largely uniform during June-August across the northern WUS, with many grid cells expecting increases of 2–4 days per month (Figures S4a–S4c, Table S1 in Supporting Information S1). Notably, projected monthly changes in CG lightning days are weak and non-robust across most of the interior Southwest, reflecting large ensemble spread and uncertainty in future directions of convective activity over this region (Figures S4a–S4d in Supporting Information S1; see also Figure 2c). These findings likely reflect the well-known uncertainties in NAM projections (e.g., Kelly & Mapes, 2010; Pascale et al., 2019; Wallace & Minder, 2024). Monthly increases in LIW-risk days, on the other hand, are concentrated in the eastern WUS and over July-August, peaking at a ∼1.5 days increase over the Colorado Plateau and Southern Rockies in August (Figures S4e–S4h, Table S2 in Supporting Information S1). Importantly, none of the ecoprovinces project a decrease in LIW-risk days in any month (Table S2 in Supporting Information S1).

3.3. Drivers of Projected CG Lightning Changes

To understand the physical drivers of the projected changes in future CG lightning days, we analyze individual changes in the thermodynamic predictor variables and the associated large-scale circulation patterns. On the

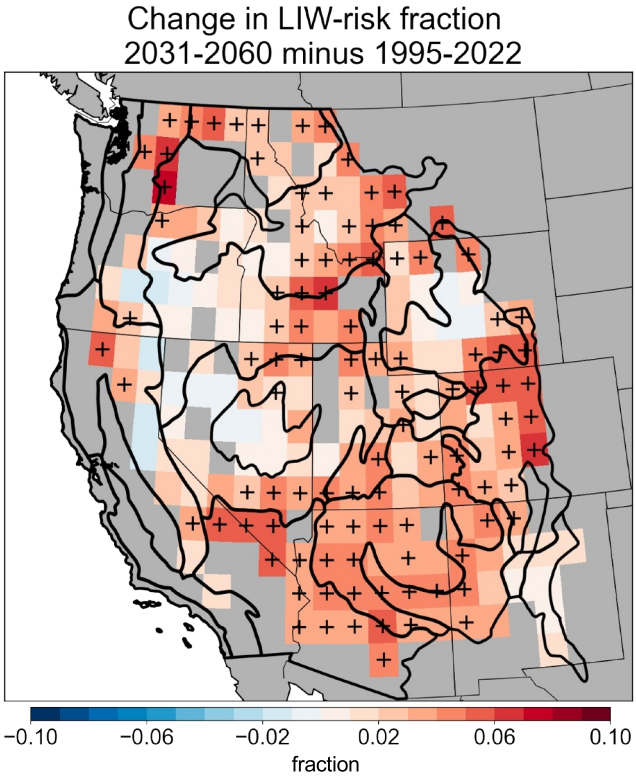

Figure 4. Ensemble-mean projected changes in the fraction of CG lightning days that are also LIW-risk days ("LIW-risk fraction") during June–September between historical (1995–2022) and mid-century (2031–2060). The change represents the arithmetic difference between the fractions in the two periods. Plus signs (dots) indicate where >75% of ensemble members agree on increases (decreases) in the fraction.

seasonal timescale, MSE_{ratio} and RH_{500} increases are robust nearly everywhere (Figures 5a and 5b). Meanwhile, robust $\Gamma_{700–500}$ increases are projected for the northern WUS (Figure 5c), overlapping with the areas of largest CG lightning increases (Figure 2a). When looking at the monthly scale, increases in the MSE_{ratio} also appear to drive the spatial patterns of CG lightning increases (Figures S5a–S5d in Supporting Information S1). For example, increases in both quantities are apparent during June–August in an arc from California northeastward to western Montana (Figures S4a–S4c, S5a–S5c in Supporting Information S1). These findings are not surprising, as the MSE_{ratio} has proven to be a simple yet effective diagnostic of convection on global scales (Noyelle et al., 2023; Y. Zhang & Boos, 2023), and was one of the most important CG lightning predictors in Kalashnikov et al. (2024). Overall increases in the MSE_{ratio} in these areas are driven by faster T_{2M} warming compared to T_{500} (the level of the free troposphere in the MSE_{ratio} calculation) and commensurate increases in Q_{2M} of up to 1 g kg^{-1} over the northern WUS (Figure S3 in Supporting Information S1). Similarly, increases in $\Gamma_{700–500}$ result from a faster warming of T_{700} relative to T_{500} (Figures S3a–S3b in Supporting Information S1). Such changes are consistent with a warming climate, as lower tropospheric warming can outpace the mid- and upper-troposphere due to land-atmosphere feedbacks (Seneviratne et al., 2010). Notably, increases in $\Gamma_{700–500}$ and RH_{500} are amplified during July–August, with increases of up to 0.4°C in $\Gamma_{700–500}$ and 5% in RH_{500} across the interior Northwest and western Great Basin (Figures S5f, S5g, S5j, and S5k in Supporting Information S1).

Projected changes in these predictors can be explained by a combination of dynamic and thermodynamic factors. Overall increases in MSE_{ratio} are associated with a warming climate, including stronger near-surface warming and an atmosphere capable of holding more water vapor due to Clausius–Clapeyron scaling. The amplified increases in MSE_{ratio} and RH_{500} across the western and northern WUS, along with weaker increases and even decreases (e.g., in RH_{500} during July–August; Figures S5f and S5g in Supporting Information S1) in parts of the interior Southwest are likely driven by changes in the strength and extent of the NAM upper-level anticyclone (Figure 6). The mean position of this high-pressure system, typically anchored over the "Four Corners" region of the interior Southwest (Figure 8a) (Adams & Comrie, 1997; Carleton, 1987), will largely remain centered over this region but experiences a notable expansion and amplification further northwest in CESM2 (Figures 6b and 6c). This is especially apparent in July–August, which represents the

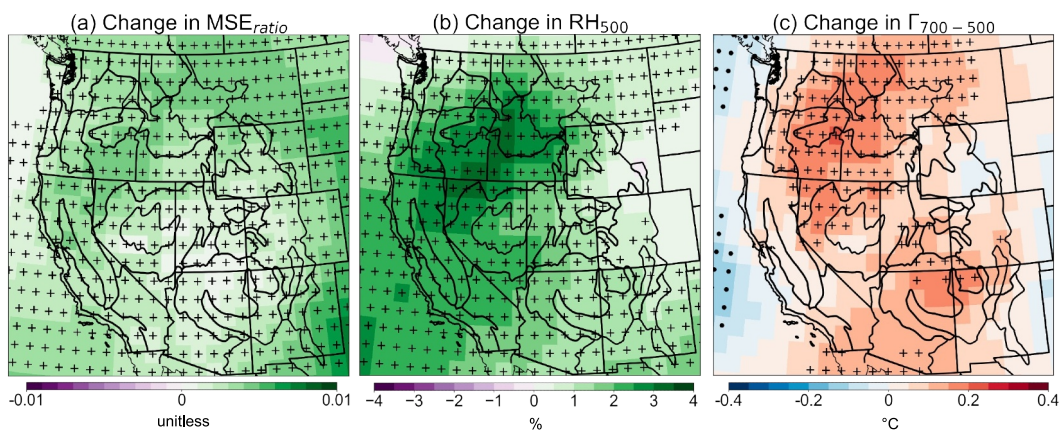

Figure 5. Ensemble-mean projected changes in CG lightning predictor variables: (a) MSE_{ratio}, (b) RH_{500}, and (c) $\Gamma_{700–500}$ between historical (1995–2022) and mid-century (2031–2060) during June-September. Plus signs (dots) indicate where >75% of ensemble members agree on increases (decreases).

10.1029/2025EF006108

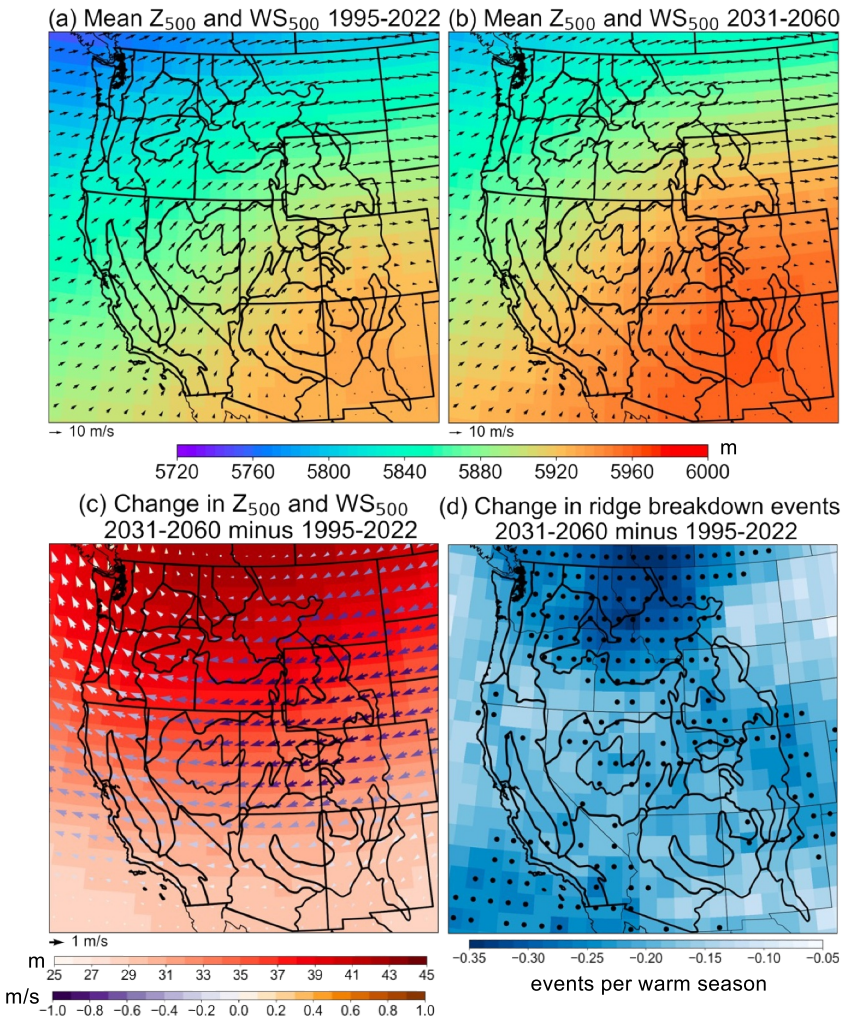

Figure 6. CESM2 ensemble-mean averages of Z_{500} and WS_{500} on all warm-season days during (a) 1995–2022 and (b) 2031–2060, and (c) ensemble-mean changes in these quantities between the two periods. (d) Ensemble-mean change in the frequency of ridge breakdown events, defined at each grid cell as $>1\sigma$ positive Z_{500} anomalies that are followed by $<0.5\sigma$ negative anomalies within 3 days. Dots indicate where >75% of ensemble members agree on decreases.

climatological peak of the NAM (Barlow et al., 1998), with Z_{500} increases exceeding 45 m in parts of the interior Northwest that substantially outpace geopotential height increases further south (Figures S6j and S6k in Supporting Information S1) similar to prior studies (e.g., Pascale et al., 2018). As a result, notable dynamical changes to the summertime large-scale WUS circulation are projected in CESM2. Mid-tropospheric monsoonal moisture transport on the western side of the NAM anticyclone appears to shift further north and west, increasingly affecting the interior Northwest and western Great Basin as reflected by increased RH_{500} (Figure 5b), with resultant increases in both CG lightning and precipitation (Figures 2a and 3c). This is corroborated by weakening westerlies, quantified by WS_{500}, by up to 1 m s^{-1} over the WUS during the warm season (Figure 6c). Consequently, "ridge breakdown" patterns that are favorable for widespread dry lightning outbreaks (see Methods) are projected to decrease in the northern WUS, likely due to fewer mid-latitude disturbances transiting the region (Figure 6d) (Brewer & Mass, 2016). A possible implication of our findings is that areas of the northern Great Basin and interior Northwest may transition to a more monsoonal thunderstorm regime, with more frequent airmass thunderstorms and accompanying precipitation under increased moisture advection. Although this could signal a reduced risk of large, simultaneous LIW outbreaks, the overall risk of sustained LIW ignition and spread is expected to rise due to increasing background temperatures, FWI, and CG lightning occurrence.

4. Discussion and Conclusions

CNN-based projections show widespread, robust increases in CG lightning days across the northern WUS during the warm season by the mid-21st century of up to 8.9 days in the Middle Rockies, while the southern WUS shows weak and non-robust increases and some decreases (Figures 2a and 2c). LIW-risk days are projected to robustly increase nearly everywhere, with the strongest increases in the Southern Rockies (+3.4 days) and Middle Rockies (+3.0 days) (Figures 2b and 2c). Areas in Utah and Arizona may still experience substantially more LIW-risk days due to increased FWI, even with minimal changes to CG lightning days. Approximately 92% of the WUS is expected to experience an increase in the LIW-risk fraction, or the ratio of LIW-risk days to all CG lightning days, driven by increased FWI (Figure 4). These findings highlight the heightened risk of LIWs due to concurrent increases in CG lightning and fire weather conditions, though uncertainties remain regarding future trajectories of CG lightning days in the NAM core. Such changes could pose challenges for the future management and suppression of LIWs, as more ignitions might be expected.

Our manuscript makes several novel contributions. To our knowledge, this work represents the first time that localized parameterizations have been applied to project CG lightning and LIW risk over the WUS. This region is prone to both deep convection in the NAM core and instances of dry lightning on the NAM periphery, which occur in conjunction with differing atmospheric conditions. These nuances may not be captured by parameterizations developed at national to global scales, necessitating our localized approach. Our results demonstrate the value of including FWI projections in future lightning assessments in contrast to prior studies, as the FWI provides context to changes in LIW risk beyond CG lightning projections alone. The inclusion of FWI results in some areas seeing increases in LIW-risk days that outpace projected increases in CG lightning days (e.g., interior Southwest), while in others, it tempers the projections of LIW risk that might be expected from increases in CG lightning in isolation (e.g., northern Great Basin). Our projections offer a new level of detail in understanding changes to near-term CG lightning and LIW-risk days over the WUS and can inform present-day policy decisions and adaptation planning. In contrast, prior studies have typically made projections using global parameterizations and for the end of the 21st century with sometimes contradictory results, leaving uncertainty in anticipated near-term trajectories of lightning and associated hazards for the WUS. For example, using global convective parameterizations, Finney et al. (2018) and Janssen et al. (2023) projected increases in total lightning (CG and in-cloud) flash rates across the WUS as part of their broader analyses, but showed different spatial patterns of changes across the region. Pérez-Invernón et al. (2023), also using a convective parameterization, projected widespread increases in total and CG lightning, as well as LIW risk factors, but their projections were limited to 2091–2095. Meanwhile, Etten-Bohm et al. (2024) and Whaley et al. (2024), using a lightning parameterization developed from the large-scale environment over the global tropics and subtropics, projected weak to no increases in total lightning occurrence over the WUS. Our findings using local-scale, machine learning-based parameterizations applied to a large ensemble climate model emphasize that future increases in lightning occurrence are likely over the WUS, are robust to internal climate variability over the northern half of the domain, and imminent in the next few decades (2031–2060) and that LIW risk will increase ubiquitously across the domain due to increasing FWI.

We have also analyzed projections of the meteorological predictor variables and large-scale circulation patterns to understand the drivers behind future CG lightning increases. MSE_{ratio} and RH_{500} are projected to increase robustly across much of the WUS, while $\Gamma_{700–500}$ increases are mainly concentrated in the northern WUS (Figure 5). The areas of largest increases in all three predictors match the areas of largest CG lightning increases, particularly in the northern and western WUS, with these increases peaking in July–August. This is likely due to warming-driven thermodynamics such as stronger near-surface heating, amplified by circulation changes like the expansion and northwestward shift of the NAM upper-level anticyclone (Figure 6). These shifts affect moisture transport reflected in increased RH_{500} across the interior Northwest and western Great Basin, leading to increased CG lightning days but also precipitation (Figure 3c). In these areas, the largest increase in risk may not be from LIW ignitions but rather hydrologic hazards such as flash flooding and slope failure from heavy rain-producing thunderstorms, particularly if affecting recently burned slopes (Touma et al., 2022).

We acknowledge several potential limitations to our analysis. First, we make projections of CG lightning days (≥1 CG flash) rather than total quantity of CG lightning flashes, and we do so at a relatively coarse $1° \times 1°$ spatial resolution. We therefore are unable to evaluate changes to lightning flash quantity on daily to seasonal scales, which could affect LIW ignition potential (e.g., Chen & Jin, 2022; Vant-Hull & Koshak, 2023) or examine finer-scale spatial changes which may have important implications in the mountainous WUS terrain (Kalashnikov,

Abatzoglou, et al., 2022). Second, we note biases between CNN-based parameterizations and observations (Figure 1) which we mitigate by assessing changes to CG lightning occurrence in the CESM2 model space, assuming similar mean biases exist in historical and future simulations. Third, our analysis is limited to one GCM with relatively high climate sensitivity and emission scenario (SSP3-7.0); we therefore constrain our projections to the mid-21st century when CESM2 global mean temperatures do not yet diverge substantially from other climate models and future emission scenarios (Fan et al., 2020; Gettelman et al., 2019; Meehl, Arblaster, et al., 2020). A comparison of modeled changes from multiple GCMs and greenhouse gas trajectories is needed to evaluate uncertainties in projections arising from structural differences among models and emissions scenarios. Nonetheless, we leverage the CESM2 large ensemble to account for projection uncertainty due to internal climate variability, which can be relatively large on regional-to-local scales and in the near-term for certain variables compared to model or scenario uncertainties (Lehner & Deser, 2023). Finally, the median FWI values used to define LIW risk herein are broadly representative within ecoprovinces but do not account for localized vegetation conditions that may alter the likelihood of CG lightning starting a wildfire. By adopting this approach, we provide projections of days conducive to LIW ignition without explicitly modeling fires themselves. Overall, our results suggest a convergence of CG lightning and fire-conducive weather in a warming climate that will broadly increase LIW risk across the WUS. Our findings can be used to assess the changing risks of thunderstorm hazards, including LIW ignitions, and inform proactive adaptation strategies.

Data Availability Statement

NLDN data are sourced from the National Centers for Environmental Information Severe Weather Data Inventory (https://www.ncei.noaa.gov/pub/data/swdi/database-csv/v2/). MERRA-2 data were acquired from NASA's Goddard Earth Sciences Data Information Services Center (GES DISC): https://disc.gsfc.nasa.gov/datasets?keywords=merra-2&page=1. GLDAS data were obtained from NASA's Land Data Assimilation System (data set: GLDASp5_domveg_VIC4.1.2_10d.nc4): https://ldas.gsfc.nasa.gov/gldas/vegetation-class-mask. CESM2-LENS2 data are publicly available for download from https://www.cesm.ucar.edu/community-projects/lens2/data-sets. Ecoprovince polygons were sourced from the US Geological Survey (https://www.sciencebase.gov/catalog/item/54244abde4b037b608f9e23d). Data sets used to perform analyses are available at the following Zenodo repository: https://doi.org/10.5281/zenodo.10685571 (Kalashnikov, 2024). Analysis code can be accessed at the following Zenodo repository: https://doi.org/10.5281/zenodo.14822736 (Kalashnikov, 2025).

Acknowledgments

We thank Vaisala, Inc. for collecting the NLDN lightning data used in this study. We thank Dr. Bor-Ting Jong for helpful comments during the GFDL internal review, and we also thank Dr. Vincent Verjans for helpful discussions regarding lightning parameterizations. We acknowledge the CESM2 Large Ensemble Community Project and supercomputing resources provided by the IBS Center for Climate Physics in South Korea. This research used resources from the Center for Institutional Research Computing at Washington State University and the Casper system provided by the National Center for Atmospheric Research (NCAR), sponsored by the National Science Foundation. This work was supported by NASA awards 80NSSC21K1603 (DAK and DS) and 80NSSC21K1501 (PCL), and by NSF awards AGS-PRF #2403765 (DAK) and OAI-2019762 (JTA). ZML acknowledges support through base funding of GFDL provided by the National Oceanic and Atmospheric Administration (NOAA). The statements, findings, conclusions, and recommendations are those of the authors and do not necessarily reflect the views of NOAA, or the U.S. Department of Commerce.

References

Abadi, M., Agarwal, A., Barham, P., Brevdo, E., Chen, Z., Citro, C., et al. (2015). TensorFlow: Large-scale machine learning on heterogeneous distributed systems. Retrieved from https://static.googleusercontent.com/media/research.google.com/en//pubs/archive/45166.pdf

Abatzoglou, J. T., Battisti, D. S., Williams, A. P., Hansen, W. D., Harvey, B. J., & Kolden, C. A. (2021a). Projected increases in western US forest fire despite growing fuel constraints. *Communications Earth & Enviornment*, *2*(1), 227. https://doi.org/10.1038/s43247-021-00299-0

Abatzoglou, J. T., & Brown, T. J. (2009). Influence of the Madden–Julian Oscillation on summertime cloud-to-ground lightning activity over the continental United States. *Monthly Weather Review*, *137*(10), 3596–3601. https://doi.org/10.1175/2009MWR3019.1

Abatzoglou, J. T., Juang, C. S., Williams, A. P., Kolden, C. A., & Westerling, A. L. (2021b). Increasing synchronous fire danger in forests of the western United States. *Geophysical Research Letters*, *48*(2), e2020GL091377. https://doi.org/10.1029/2020GL091377

Abatzoglou, J. T., Kolden, C. A., Balch, J. K., & Bradley, B. A. (2016). Controls on interannual variability in lightning-caused fire activity in the western US. *Environmental Research Letters*, *11*(4), 045005. https://doi.org/10.1088/1748-9326/11/4/045005

Abatzoglou, J. T., Williams, A. P., & Barbero, R. (2019). Global emergence of anthropogenic climate change in fire weather indices. *Geophysical Research Letters*, *46*(1), 326–336. https://doi.org/10.1029/2018GL080959

Abolafia-Rosenzweig, R., He, C., & Chen, F. (2022). Winter and spring climate explains a large portion of interannual variability and trend in western U.S. summer fire burned area. *Environmental Research Letters*, *17*(5), 054030. https://doi.org/10.1088/1748-9326/ac6886

Adams, D. K., & Comrie, A. C. (1997). The North American monsoon. *Bulletin of the American Meteorological Society*, *78*(10), 2197–2213. https://doi.org/10.1175/1520-0477(1997)078<2197:TNAM>2.0.CO;2

Alexander, G. W. (1927). Lightning storms and forest fires in the state of Washington. *Monthly Weather Review*, *55*(3), 122–129. https://doi.org/10.1175/1520-0493(1927)55<122:LSAFFI>2.0.CO;2

Allen, D. J., & Pickering, K. E. (2002). Evaluation of lightning flash rate parameterizations for use in a global chemical transport model. *Journal of Geophysical Research*, *107*(D23), ACH15-1–ACH15-21. https://doi.org/10.1029/2002JD002066

Baño-Medina, J., Manzanas, R., & Gutiérrez, J. M. (2021). On the suitability of deep convolutional neural networks for continental-wide downscaling of climate change projections. *Climate Dynamics*, *57*(11–12), 2941–2951. https://doi.org/10.1007/s00382-021-05847-0

Barbero, R., Abatzoglou, J. T., Steel, E. A., & K Larkin, N. (2014). Modeling very large-fire occurrences over the continental United States from weather and climate forcing. *Environmental Research Letters*, *9*(12), 124009. https://doi.org/10.1088/1748-9326/9/12/124009

Barlow, M., Nigam, S., & Berbery, E. H. (1998). Evolution of the North American monsoon system. *Journal of Climate*, *11*(9), 2238–2257. https://doi.org/10.1175/1520-0442(1998)011<2238:EOTNAM>2.0.CO;2

Barros, A. M. G., Day, M. A., Preisler, H. K., Abatzoglou, J. T., Krawchuk, M. A., Houtman, R., & Ager, A. A. (2021). Contrasting the role of human- and lightning-caused wildfires on future fire regimes on a Central Oregon landscape. *Environmental Research Letters*, *16*(6), 064081. https://doi.org/10.1088/1748-9326/ac03da

Beucler, T., Gentine, P., Yuval, J., Gupta, A., Peng, L., Lin, J., et al. (2024). Climate-invariant machine learning. *Science Advances*, *10*(6), adj7250. https://doi.org/10.1126/sciadv.adj7250

Bourgault, P., Huard, D., Smith, T. J., Logan, T., Aoun, A., Lavoie, J., et al. (2023). xclim: Xarray-based climate data analytics. *Journal of Open Source Software*, *8*(85), 5415. https://doi.org/10.21105/joss.05415

Brewer, M. C., & Mass, C. F. (2016). Projected changes in western U.S. large-scale summer synoptic circulations and variability in CMIP5 models. *Journal of Climate*, *29*(16), 5965–5978. https://doi.org/10.1175/JCLI-D-15-0598.1

Brown, E. K., Wang, J., & Feng, Y. (2021). US wildfire potential: A historical view and future projection using high-resolution climate data. *Environmental Research Letters*, *16*(3), 034060. https://doi.org/10.1088/1748-9326/aba868

Burke, M., Childs, M. L., de la Cuesta, B., Qiu, M., Li, J., Gould, C. F., et al. (2023). The contribution of wildfire to $PM_{2.5}$ trends in the USA. *Nature*, *622*(7984), 761–766. https://doi.org/10.1038/s41586-023-06522-6

Cannon, A. J. (2018). Multivariate quantile mapping bias correction: An N-dimensional probability density function transform for climate model simulations of multiple variables. *Climate Dynamics*, *50*(1–2), 31–49. https://doi.org/10.1007/s00382-017-3580-6

Cannon, A. J., Alford, H., Shrestha, R. R., Kirchmeier-Young, M. C., & Najafi, M. R. (2022). Canadian Large ensembles adjusted dataset version 1 (CanLEADv1): Multivariate bias-corrected climate model outputs for terrestrial modelling and attribution studies in North America. *Geoscience Data Journal*, *9*(2), 288–303. https://doi.org/10.1002/gdj3.142

Cannon, A. J., Sobie, S. R., & Murdock, T. Q. (2015). Bias correction of GCM precipitation by quantile mapping: How well do methods preserve changes in quantiles and extremes? *Journal of Climate*, *28*(17), 6938–6959. https://doi.org/10.1175/JCLI-D-14-00754.1

Carleton, A. M. (1987). Summer circulation climate of the American southwest, 1945–1984. *Annals of the Association of American Geographers*, *77*(4), 619–634. https://doi.org/10.1111/j.1467-8306.1987.tb00184.x

Charn, A. B., & Parishani, H. (2021). Predictive proxies of present and future lightning in a superparameterized model. *Journal of Geophysical Research: Atmospheres*, *126*(17), e2021JD035461. https://doi.org/10.1029/2021jd035461

Chen, B., & Jin, Y. (2022). Spatial patterns and drivers for wildfire ignitions in California. *Environmental Research Letters*, *17*(5), 055004. https://doi.org/10.1088/1748-9326/ac60da

Chen, Y., Romps, D. M., Seeley, J. T., Veraverbeke, S., Riley, W. J., Mekonnen, Z. A., & Randerson, J. T. (2021). Future increases in Arctic lightning and fire risk for permafrost carbon. *Nature Climate Change*, *11*(5), 404–410. https://doi.org/10.1038/s41558-021-01011-y

Cheng, W.-Y., Kim, D., Henderson, S., Ham, Y.-G., Kim, J.-H., & Holzworth, R. H. (2024). Machine learning based lightning parameterizations for CONUS. *Artificial Intelligence for the Earth Systems*, *3*(2), 1–18. https://doi.org/10.1175/AIES-D-23-0024.1

Clark, S. K., Ward, D. S., & Mahowald, N. M. (2017). Parameterization-based uncertainty in future lightning flash density. *Geophysical Research Letters*, *44*(6), 2893–2901. https://doi.org/10.1002/2017GL073017

Danabasoglu, G., Lamarque, J.-F., Bacmeister, J., Bailey, D. A., DuVivier, A. K., Edwards, J., et al. (2020). The community earth system model version 2 (CESM2). *Journal of Advances in Modeling Earth Systems*, *12*(2), e2019MS001916. https://doi.org/10.1029/2019ms001916

Deser, C., Knutti, R., Solomon, S., & Phillips, A. S. (2012). Communication of the role of natural variability in future North American climate. *Nature Climate Change*, *2*(11), 775–779. https://doi.org/10.1038/nclimate1562

Di Giuseppe, F., Rémy, S., Pappenberger, F., & Wetterhall, F. (2018). Using the Fire Weather Index (FWI) to improve the estimation of fire emissions from fire radiative power (FRP) observations. *Atmospheric Chemistry and Physics*, *18*(8), 5359–5370. https://doi.org/10.5194/acp-18-5359-2018

Etten-Bohm, M., Schumacher, C., Xu, Y., & Funk, A. (2024). Projection of global future lightning occurrence using only large-scale environmental variables in CAM5. *ESS Open Archive*. https://doi.org/10.22541/au.171052461.15341485/v1

Etten-Bohm, M., Yang, J., Schumacher, C., & Jun, M. (2021). Evaluating the relationship between lightning and the large-scale environment and its use for lightning prediction in global climate models. *Journal of Geophysical Research: Atmospheres*, *126*(5), e2020JD033990. https://doi.org/10.1029/2020jd033990

Fan, X., Duan, Q., Shen, C., Wu, Y., & Xing, C. (2020). Global surface air temperatures in CMIP6: Historical performance and future changes. *Environmental Research Letters*, *15*(10), 104056. https://doi.org/10.1088/1748-9326/abb051

Finney, D. L., Doherty, R. M., Wild, O., Stevenson, D. S., MacKenzie, I. A., & Blyth, A. M. (2018). A projected decrease in lightning under climate change. *Nature Climate Change*, *8*(3), 210–213. https://doi.org/10.1038/s41558-018-0072-6

Fusco, E. J., Finn, J. T., Abatzoglou, J. T., Balch, J. K., Dadashi, S., & Bradley, B. A. (2019). Detection rates and biases of fire observations from MODIS and agency reports in the conterminous United States. *Remote Sensing of Environment*, *220*, 30–40. https://doi.org/10.1016/j.rse.2018.10.028

Gallo, C., Eden, J. M., Dieppois, B., Drobyshev, I., Fulé, P. Z., San-Miguel-Ayanz, J., & Blackett, M. (2023). Evaluation of CMIP6 model performances in simulating fire weather spatiotemporal variability on global and regional scales. *Geoscientific Model Development*, *16*(10), 3103–3122. https://doi.org/10.5194/gmd-16-3103-2023

Gelaro, R., McCarty, W., Suárez, M. J., Todling, R., Molod, A., Takacs, L., et al. (2017). The Modern-Era retrospective analysis for research and applications, version 2 (MERRA-2). *Journal of Climate*, *30*(13), 5419–5454. https://doi.org/10.1175/JCLI-D-16-0758.1

Gettelman, A., Hannay, C., Bacmeister, J. T., Neale, R. B., Pendergrass, A. G., Danabasoglu, G., et al. (2019). High climate sensitivity in the community earth system model version 2 (CESM2). *Geophysical Research Letters*, *46*(14), 8329–8337. https://doi.org/10.1029/2019GL083978

Goss, M., Swain, D. L., Abatzoglou, J. T., Sarhadi, A., Kolden, C. A., Williams, A. P., & Diffenbaugh, N. S. (2020). Climate change is increasing the likelihood of extreme autumn wildfire conditions across California. *Environmental Research Letters*, *15*(9), 094016. https://doi.org/10.1088/1748-9326/ab83a7

He, K., Zhang, X., Ren, S., & Sun, J. (2015). Delving deep into rectifiers: Surpassing human-level performance on ImageNet classification. In *Proceedings of the IEEE international conference on computer vision (ICCV)* (pp. 1026–1034). Retrieved from https://openaccess.thecvf.com/content_iccv_2015/html/He_Delving_Deep_into_ICCV_2015_paper.html

Janssen, T. A. J., Jones, M. W., Finney, D., van der Werf, G. R., van Wees, D., Xu, W., & Veraverbeke, S. (2023). Extratropical forests increasingly at risk due to lightning fires. *Nature Geoscience*, *16*(12), 1136–1144. https://doi.org/10.1038/s41561-023-01322-z

Kalashnikov, D. A. (2024). Supporting datasets for CNNs-lightning prediction paper (Version 1) [Dataset]. *Zenodo*. https://doi.org/10.5281/zenodo.10685571

Kalashnikov, D. A. (2025). Code for CESM2 lightning projections (version 2) [Software]. *Zenodo*. https://doi.org/10.5281/zenodo.14822736

Kalashnikov, D. A., Abatzoglou, J. T., Loikith, P. C., Nauslar, N. J., Bekris, Y., & Singh, D. (2023). Lightning-ignited wildfires in the western United States: Ignition precipitation and associated environmental conditions. *Geophysical Research Letters*, *50*(16), e2023GL103785. https://doi.org/10.1029/2023gl103785

Kalashnikov, D. A., Abatzoglou, J. T., Nauslar, N. J., Swain, D. L., Touma, D., & Singh, D. (2022b). Meteorological and geographical factors associated with dry lightning in central and northern California. *Environmental Research: Climate*, *1*(2), 025001. https://doi.org/10.1088/2752-5295/ac84a0

Kalashnikov, D. A., Davenport, F. V., Labe, Z. M., Loikith, P. C., Abatzoglou, J. T., & Singh, D. (2024). Predicting cloud-to-ground lightning in the western United States from the large-scale environment using explainable neural networks. *Journal of Geophysical Research: Atmospheres*, *129*(22), e2024JD042147. https://doi.org/10.1029/2024JD042147

Kalashnikov, D. A., Loikith, P. C., Catalano, A. J., Waliser, D. E., Lee, H., & Abatzoglou, J. T. (2020). A 30-yr climatology of meteorological conditions associated with lightning days in the interior western United States. *Journal of Climate*, *33*(9), 3771–3785. https://doi.org/10.1175/JCLI-D-19-0564.1

Kalashnikov, D. A., Schnell, J. L., Abatzoglou, J. T., Swain, D. L., & Singh, D. (2022a). Increasing co-occurrence of fine particulate matter and ground-level ozone extremes in the western United States. *Science Advances*, *8*(1), eabi9386. https://doi.org/10.1126/sciadv.abi9386

Kelly, P., & Mapes, B. (2010). Land surface heating and the North American monsoon anticyclone: Model evaluation from diurnal to seasonal. *Journal of Climate*, *23*(15), 4096–4106. https://doi.org/10.1175/2010JCLI3332.1

Kirchmeier-Young, M. C., Zwiers, F. W., Gillett, N. P., & Cannon, A. J. (2017). Attributing extreme fire risk in Western Canada to human emissions. *Climatic Change*, *144*(2), 365–379. https://doi.org/10.1007/s10584-017-2030-0

Krause, A., Kloster, S., Wilkenskjeld, S., & Paeth, H. (2014). The sensitivity of global wildfires to simulated past, present, and future lightning frequency. *Journal of Geophysical Research: Biogeosciences*, *119*(3), 312–322. https://doi.org/10.1002/2013JG002502

Lehner, F., & Deser, C. (2023). Origin, importance, and predictive limits of internal climate variability. *Environmental Research: Climate*, *2*(2), 023001. https://doi.org/10.1088/2752-5295/accf30

Lehner, F., Deser, C., Maher, N., Marotzke, J., Fischer, E. M., Brunner, L., et al. (2020). Partitioning climate projection uncertainty with multiple large ensembles and CMIP5/6. *Earth System Dynamics*, *11*(2), 491–508. https://doi.org/10.5194/esd-11-491-2020

Li, Y., Mickley, L. J., Liu, P., & Kaplan, J. O. (2020). Trends and spatial shifts in lightning fires and smoke concentrations in response to 21st century climate over the national forests and parks of the western United States. *Atmospheric Chemistry and Physics*, *20*(14), 8827–8838. https://doi.org/10.5194/acp-20-8827-2020

Liu, J. C., Mickley, L. J., Sulprizio, M. P., Dominici, F., Yue, X., Ebisu, K., et al. (2016). Particulate air pollution from wildfires in the western US under climate change. *Climatic Change*, *138*(3), 655–666. https://doi.org/10.1007/s10584-016-1762-6

Liu, N., Liu, C., & Tissot, P. E. (2022). Relative importance of large-scale environmental variables to the world-wide variability of thunderstorms. *Journal of Geophysical Research: Atmospheres*, *127*(17), e2021JD036065. https://doi.org/10.1029/2021jd036065

Magi, B. I. (2015). Global lightning parameterization from CMIP5 climate model output. *Journal of Atmospheric and Oceanic Technology*, *32*(3), 434–452. https://doi.org/10.1175/JTECH-D-13-00261.1

McClure, C. D., & Jaffe, D. A. (2018). US particulate matter air quality improves except in wildfire-prone areas. *Proceedings of the National Academy of Sciences of the United States of America*, *115*(31), 7901–7906. https://doi.org/10.1073/pnas.1804353115

McGinnis, S., Kessenich, L., Mearns, L., Cullen, A., Podschwit, H., & Bukovsky, M. (2023). Future regional increases in simultaneous large Western USA wildfires. *International Journal of Wildland Fire*, *32*(9), 1304–1314. https://doi.org/10.1071/WF22107

Meehl, G. A., Arblaster, J. M., Bates, S., Richter, J. H., Tebaldi, C., Gettelman, A., et al. (2020a). Characteristics of future warmer base states in CESM2. *Earth and Space Science*, *7*(9), e2020EA001296. https://doi.org/10.1029/2020ea001296

Meehl, G. A., Shields, C., Arblaster, J. M., Annamalai, H., & Neale, R. (2020b). Intraseasonal, seasonal, and interannual characteristics of regional monsoon simulations in CESM2. *Journal of Advances in Modeling Earth Systems*, *12*(6), e2019MS001962. https://doi.org/10.1029/2019ms001962

Molina, M. J., Gagne, D. J., & Prein, A. F. (2021). A benchmark to test generalization capabilities of deep learning methods to classify severe convective storms in a changing climate. *Earth and Space Science*, *8*(9), e2020EA001490. https://doi.org/10.1029/2020ea001490

Molina, M. J., O'Brien, T. A., Anderson, G., Ashfaq, M., Bennett, K. E., Collins, W. D., et al. (2023). A review of recent and emerging machine learning applications for climate variability and weather phenomena. *Artificial Intelligence for the Earth Systems*, *2*(4). https://doi.org/10.1175/aies-d-22-0086.1

Nauslar, N., Kaplan, M., Wallmann, J., & Brown, T. (2013). A forecast procedure for dry thunderstorms. *Journal of Operational Meteorology*, *1*(17), 200–214. https://doi.org/10.15191/nwajom.2013.0117

Noyelle, R., Zhang, Y., Yiou, P., & Faranda, D. (2023). Maximal reachable temperatures for Western Europe in current climate. *Environmental Research Letters*, *18*(9), 094061. https://doi.org/10.1088/1748-9326/acf679

Pascale, S., Carvalho, L. M. V., Adams, D. K., Castro, C. L., & Cavalcanti, I. F. A. (2019). Current and future variations of the monsoons of the Americas in a warming climate. *Current Climate Change Reports*, *5*(3), 125–144. https://doi.org/10.1007/s40641-019-00135-w

Pascale, S., Kapnick, S. B., Bordoni, S., & Delworth, T. L. (2018). The influence of CO_2 forcing on North American Monsoon moisture surges. *Journal of Climate*, *31*(19), 7949–7968. https://doi.org/10.1175/JCLI-D-18-0007.1

Pérez-Invernón, F. J., Gordillo-Vázquez, F. J., Huntrieser, H., & Jöckel, P. (2023). Variation of lightning-ignited wildfire patterns under climate change. *Nature Communications*, *14*(1), 739. https://doi.org/10.1038/s41467-023-36500-5

Pitie, F., Kokaram, A. C., & Dahyot, R. (2005). N-dimensional probability density function transfer and its application to color transfer. In *Tenth IEEE international conference on computer vision (ICCV'05) volume 1*. IEEE. https://doi.org/10.1109/iccv.2005.166

Price, C., & Rind, D. (1992). A simple lightning parameterization for calculating global lightning distributions. *Journal of Geophysical Research*, *97*(D9), 9919–9933. https://doi.org/10.1029/92JD00719

Price, C., & Rind, D. (1994). The impact of a 2x CO_2 climate on lightning-caused fires. *Journal of Climate*, *7*(10), 1484–1494. https://doi.org/10.1175/1520-0442(1994)007<1484:TIOACC>2.0.CO;2

Rao, K., Williams, A. P., Diffenbaugh, N. S., Yebra, M., Bryant, C., & Konings, A. G. (2023). Dry live fuels increase the likelihood of lightning-caused fires. *Geophysical Research Letters*, *50*(15), e2022GL100975. https://doi.org/10.1029/2022GL100975

Rodgers, K. B., Lee, S.-S., Rosenbloom, N., Timmermann, A., Danabasoglu, G., Deser, C., et al. (2021). Ubiquity of human-induced changes in climate variability. *Earth System Dynamics*, *12*(4), 1393–1411. https://doi.org/10.5194/esd-12-1393-2021

Romps, D. M. (2019). Evaluating the future of lightning in cloud-resolving models. *Geophysical Research Letters*, *46*(24), 14863–14871. https://doi.org/10.1029/2019GL085748

Romps, D. M., Seeley, J. T., Vollaro, D., & Molinari, J. (2014). Projected increase in lightning strikes in the United States due to global warming. *Science*, *346*(6211), 851–854. https://doi.org/10.1126/science.1259100

Rorig, M. L., & Ferguson, S. A. (1999). Characteristics of lightning and wildland fire ignition in the pacific northwest. *Journal of Applied Meteorology and Climatology*, *38*(11), 1565–1575. https://doi.org/10.1175/1520-0450(1999)038<1565:COLAWF>2.0.CO;2

Schultz, C. J., Nauslar, N. J., Wachter, J. B., Hain, C. R., & Bell, J. R. (2019). Spatial, temporal, and electrical characteristics of lightning in reported lightning-initiated wildfire events. *Fire*, *2*(2), 18. https://doi.org/10.3390/fire2020018

Seneviratne, S. I., Corti, T., Davin, E. L., Hirschi, M., Jaeger, E. B., Lehner, I., et al. (2010). Investigating soil moisture–climate interactions in a changing climate: A review. *Earth-Science Reviews*, *99*(3–4), 125–161. https://doi.org/10.1016/j.earscirev.2010.02.004

Short, K. C. (2022). *Spatial wildfire occurrence data for the United States, 1992–2020 [FPA_FOD_20221014]* (6th ed.). Forest Service Research Data Archive. https://doi.org/10.2737/RDS-2013-0009.6

Tebaldi, C., Dorheim, K., Wehner, M., & Leung, R. (2021). Extreme metrics from large ensembles: Investigating the effects of ensemble size on their estimates. *Earth System Dynamics*, *12*(4), 1427–1501. https://doi.org/10.5194/esd-12-1427-2021

Toms, B. A., Barnes, E. A., & Ebert-Uphoff, I. (2020). Physically interpretable neural networks for the geosciences: Applications to earth system variability. *Journal of Advances in Modeling Earth Systems*, *12*(9), e2019MS002002. https://doi.org/10.1029/2019ms002002

Touma, D., Hurrell, J. W., Tye, M. R., & Dagon, K. (2023). The impact of stratospheric aerosol injection on extreme fire weather risk. *Earth's Future*, *11*(6), e2023EF003626. https://doi.org/10.1029/2023ef003626

Touma, D., Stevenson, S., Swain, D. L., Singh, D., Kalashnikov, D. A., & Huang, X. (2022). Climate change increases risk of extreme rainfall following wildfire in the western United States. *Science Advances*, *8*(13), eabm0320. https://doi.org/10.1126/sciadv.abm0320

United States Forest Service (USFS). (1995). Description of the ecoregions of the United States. 108

Urbieta, I. R., Zavala, G., Bedia, J., Gutiérrez, J. M., Miguel-Ayanz, J. S., Camia, A., et al. (2015). Fire activity as a function of fire–weather seasonal severity and antecedent climate across spatial scales in southern Europe and Pacific western USA. *Environmental Research Letters*, *10*(11), 114013. https://doi.org/10.1088/1748-9326/10/11/114013

Vant-Hull, B., & Koshak, W. (2023). Spatial structure of lightning and precipitation associated with lightning-caused wildfires in the central to eastern United States. *Fire*, *6*(7), 262. https://doi.org/10.3390/fire6070262

van Wagner, C. E. (1987). *Development and structure of the Canadian forest fire weather index system* (Vol. 35). Canadian Forestry Service, Forestry Technical Report.

Verjans, V., & Franzke, C. L. E. (2025). Development of a data-driven lightning scheme for implementation in global climate models. *Journal of Advances in Modeling Earth Systems*, *17*(2), e2024MS004464. https://doi.org/10.1029/2024MS004464

Wallace, B., & Minder, J. R. (2024). The North American Monsoon precipitation response to climate warming at convection-permitting scales. *Climate Dynamics*, *62*(1), 497–524. https://doi.org/10.1007/s00382-023-06920-6

Werth, P., & Ochoa, R. (1993). The evaluation of Idaho wildfire growth using the Haines index. *Weather and Forecasting*, *8*(2), 223–234. https://doi.org/10.1175/1520-0434(1993)008<0223:TEOIWG>2.0.CO;2

Whaley, C., Etten-Bohm, M., Schumacher, C., Akingunola, A., Arora, V., Cole, J., et al. (2024). A new lightning scheme in Canada's Atmospheric Model, CanAM5.1: Implementation, evaluation, and projections of lightning and fire in future climates. *Geoscientific Model Development*, *17*(18), 7141–7155. https://doi.org/10.5194/gmd-17-7141-2024

Yu, G., Feng, Y., Wang, J., & Wright, D. B. (2023). Performance of fire danger indices and their utility in predicting future wildfire danger over the conterminous United States. *Earth's Future*, *11*(11), e2023EF003823. https://doi.org/10.1029/2023EF003823

Zhang, D., Wang, W., Xi, Y., Bi, J., Hang, Y., Zhu, Q., et al. (2023). Wildland fires worsened population exposure to $PM_{2.5}$ pollution in the contiguous United States. *Environmental Science & Technology*, *57*(48), 19990–19998. https://doi.org/10.1021/acs.est.3c05143

Zhang, Y., & Boos, W. R. (2023). An upper bound for extreme temperatures over midlatitude land. *Proceedings of the National Academy of Sciences of the United States of America*, *120*(12), e2215278120. https://doi.org/10.1073/pnas.2215278120